RESEARCH ARTICLE
doi:10.59236/geomorphica.v2i1.39

GEOMORPHICA

Non-contemporaneity of flow events as a control on the morphology and sedimentary character of ephemeral tributary junctions

Daniel Cadol * [1], **Sharllyn Pimentel** [1,2], **David Varyu** [3], **Jonathan B. Laronne** [4]

[1]Department of Earth & Environmental Science, New Mexico Institute of Mining and Technology, Socorro, USA, [2]Dudek, Santa Fe, USA, [3]US Bureau of Reclamation, Denver, USA, [4]Ben Gurion University of the Negev, Beer Sheva, Israel

Author contributions: *Conceptualization*: J.B.L. *Data curation*: S.P. *Funding acquisition*: D.V. *Investigation*: D.C., S.P., D.V., and J.B.L. *Methodology*: D.C. and J.B.L. *Project Administration*: D.V. *Visualization*: S.P. *Writing - Original Draft*: D.C., S.P., and J.B.L. *Writing - Review & Editing*: D.C. and J.B.L.

Abstract River confluence geometry, dynamics, and sedimentology have predominantly been studied from the confluence downstream. Having also identified a paucity of literature on confluences of ephemeral streams, we concentrated our observations on the topography, sedimentary character, and morphologic changes that occurred during two monsoon seasons at ephemeral confluences with the Rio Grande in central New Mexico, USA. We quantified how trunk and tributary water discharge modified the junction and lowermost reach of the tributary through deposition and subsequent erosion. By excavating the sedimentary deposits, we found evidence of recirculatory deposition in the confluence mouth when only the trunk confluent flowed, and coarse bar deposition when flow was dominated by the smaller, ephemeral confluent. Trunk sediments deposited in the ephemeral branch exhibited parallel as well as cross stratification, with thicknesses decreasing upstream from the junction. Tributaries with wide junction mouths at the confluence hosted more extensive low-energy flow zones that promoted deposition of trunk river sediment, diverting and temporarily storing sediment during high trunk flows. Larger flow events in the tributaries then dissected the prior confluence junction deposits. The nature of these eddy and slackwater deposits and their resultant topographies are ephemeral, but with expected hydraulic and ecological consequences.

Received:
May 27, 2024
Accepted:
July 18, 2025
Published:
September 22, 2025

1 Introduction

In dryland regions, human development classically occurs along perennial rivers that originate in nearby mountains. These large, perennial or nearly perennial streams typically have abundant ephemeral tributaries, which flow only rarely but deliver large sediment loads when they do (Stark et al., 2024), complicating sediment and water management on the trunk river (also called the mainstem). The junctions where the ephemeral tributaries join the trunk river are morphologically dynamic (Bourke and Pickup, 1999), in part due to the different timing of flows. For example, in the mid-Rio Grande in New Mexico, USA, trunk river flows peak during spring snowmelt, but ephemeral tributaries only produce flow during flash floods of the summer monsoon, when the trunk river is at its lowest flow (Stark et al., 2021). This behavior, previously referred to as non-coincident flows (Reid et al., 1989) or asynchronous tributary activities (Bourke and Pickup, 1999), may produce morphosedimentary characteristics with different ecological or management implications than tributary confluences in perennial systems (Vyverberg, 2010).

River confluences have been studied for the past half century (Rhoads, 2020) in various geological settings (e.g., Stokes and Mather, 2015), mainly concentrating on confluence hydrodynamics such as momentum ratios, turbulence, and coherent flow structures (Bradbrook et al., 2000; Rhoads and Sukhodolov, 2004; Boyer et al., 2006; Schindfessel et al., 2017; Sukhodolov et al., 2017; Azma and Zhang, 2020; Sabrina et al., 2021; Canelas et al., 2022; Duguay et al., 2022). Other themes of investigation include confluence channel size and shape (Ashmore, 1982), spatial mobility (Dixon et al., 2018), sediment characteristics (Best, 1988; Biron et al., 1993) and their dependence on confluence angle, symmetry, sediment texture (Mosley, 1976; Best

*Corresponding author: daniel.cadol@nmt.edu

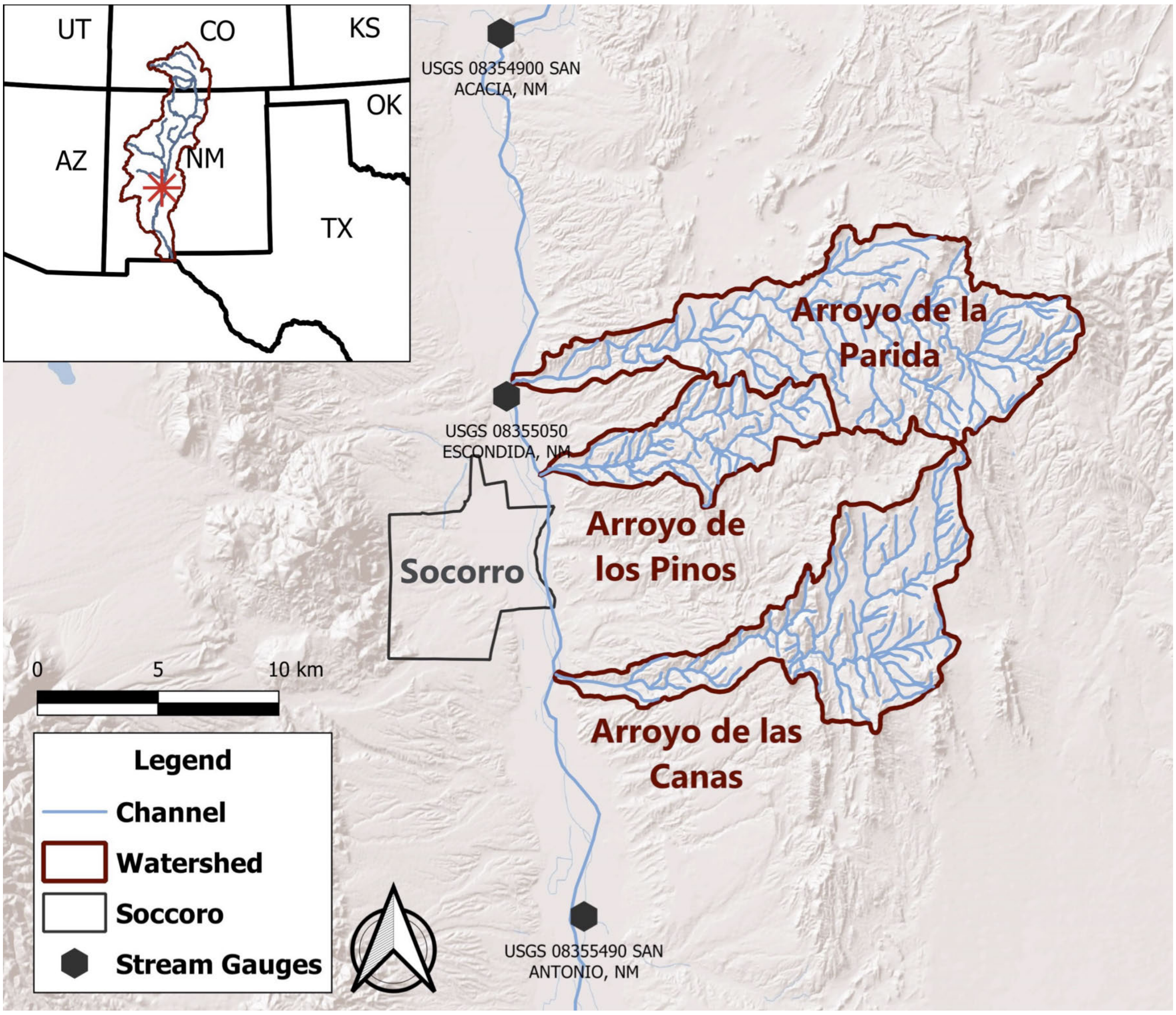

Figure 1 The watersheds of the three arroyos and their confluence with the Rio Grande near Socorro, New Mexico (NM). The local United States Geological Survey (USGS) stream gauges are also shown.

and Reid, 1984; Rhoads et al., 2009; Leite Ribeiro, 2011; Leite Ribeiro et al., 2012a), the ratio of confluent to trunk slopes (Pelletier et al., 2025), and the relative water/sediment discharges of the tributary and trunk streams (Mosley, 1976; Rhoads et al., 2009; Liu et al., 2015; Bombar and Cardoso, 2020). Recent studies have also directed attention to engineering methods to decrease the depth of confluence scour holes (Ali et al., 2019) and increase tributary width, thereby intensifying habitat heterogeneity (Rice et al., 2008; Milner et al., 2019).

A vast literature is available on tributary confluences as a source of information on slackwater deposits as evidence of past floods in the trunk stream. These efforts began in the past century (e.g., McKee, 1938; Baker et al., 1983), with interest continuing to the present (Baker, 2008; Toonen et al., 2019; Baker et al., 2022). Although megafloods rarely occur, their magnitude and internal processes can be deciphered from the character of the relevant confluence deposits (Carling, 2013). Tributary slackwater deposits have been described in various climatic settings, ranging from hyper-arid and arid (Greenbaum et al., 1998, 2000) to humid (Zhang et al., 2012). However, few have viewed river confluences as a whole in such a broad geo-hydroclimatologic framework (Benda et al., 2004a).

When there are significant flow differences between trunk rivers and their ephemeral tributaries, there is a high potential for flow upstream into the tributary from the trunk during a flood, smaller but identical to a megaflood back-flooding a tributary and leaving a slackwater deposit. Few studies have concentrated on the tributary channels upstream of the confluence, with exceptions concerning (i) tributary mouth bars with the associated avalanche faces formed at the mouth of the tributary (Best and Rhoads, 2008), (ii) situations where the scour hole progresses upstream into the tributary (e.g., Ghobadian, 2012), and (iii) the previously mentioned dating of slackwater deposits located in tributaries (Benito et al., 2003; Unde and Dhakal, 2009). We are aware of the existence of a single, though unavailable, experimental study on ephemeral stream confluence sedimentation and hydraulics (Unpublished Dissertation by C Thornes, 1991, Hertford College, University of Oxford; cited in Thornes, 1994).

Arid region confluences have been noted as unique by numerous researchers. Early observations remarked on the prevalence of nearly perpendicular junction angles (Miller, 1958). Schumm (1961) described the confluences of various ephemeral channels, including that of the smaller Arroyo Frijoles into the Arroyo Calabasas near Santa Fe, New Mexico. While the

Table 1 Confluence character of the studied tributaries.

Tributary	Catchment area [km^2]	Junction angle [°]	Width [m]	Slope [%]	Comments
Arroyo de los Pinos	32	90	30	1.2	Levees at drain crossing
Arroyo de la Parida	102	60	40	1.2	Widened to 100 m at the mouth
Arroyo de las Cañas	69	110 d/s* 55 u/s*	10 d/s* 30 u/s*	1.5	Two distributaries

*d/s – downstream branch, u/s – upstream branch

ephemeral Frijoles tributary remained dry, the larger Calabasas scoured a bar previously deposited by the Arroyo de los Frijoles, leaving the Frijoles bed perched high above the Calabasas. This study identified the non-contemporaneity of flow and sediment transport in the tributaries and the trunk stream, a phenomenon also recognized in arid portions of Australia (Bourke and Pickup, 1999) and Africa (Reid and Frostick, 2011), where mouth bars across the dry tributaries were observed. Other fine-grained sediment deposits at tributary mouths in arid portions of Arizona, USA (Wertz, 1966), and India (Unde and Dhakal, 2009) likewise suggest instances in the past where the trunk flow dominated the confluence and produced slackwater deposits in the tributary mouth, although not a fully formed bar. Finally, confluence effects on arid region trunk rivers are also widely reported, for example, the considerable sedimentary effect exerted downstream of ephemeral junctions along the Todd River, in Australia (Bourke and Pickup, 1999), and the Rio Chama, in the Rio Grande basin (Swanson and Meyer, 2014).

In this study, we focus on characterizing the confluence and near upstream tributary areas of three ephemeral tributaries of the mid-Rio Grande in New Mexico, USA, determining how their planform, junction angle, and discharge ratio contribute to the confluence morphology and sedimentology over time.

2 Study sites

The three study arroyos differ with regard to basin size, geology, channel bed grain size, and anthropogenic influences (Table 1). Therefore, processes that dominate the sediment dynamics at one site may not be as influential at others. The three arroyos have been anthropogenically modified to either alleviate lateral migration of the Rio Grande (Arroyo de las Cañas), support ecological restoration (Arroyo de la Parida; Posner, 2021), or prevent lateral migration of the tributary into an agricultural drain (Arroyo de los Pinos). Different morphological responses at each confluence are caused by the variability of sediment supply and by the localized runoff events that generate unique flow histories in each watershed.

The Arroyo de los Pinos is located south of the Arroyo de la Parida and north of the Arroyo de las Cañas (Figure 1). The upper drainage areas of these tributaries are formed in Paleozoic bedrock, mainly limestones and sandstones. Plio-Pleistocene alluvium and colluvium underlie the lower ~5 km of the basins, and Holocene mud, sand, and gravel dominate the outlets. The climate is semiarid, receiving ~250 mm of average annual rainfall. The majority of the rain occurs during the summer monsoon season. Thunderstorm cells have been observed to generate floods when moving in any cardinal direction, with particularly large floods associated with down-basin (westward) storm motion. These watersheds are at the northern edge of the Chihuahuan Desert, host to desert shrubs and cacti such as creosote, mesquite, cholla, tarbrush, prickly pear, and ocotillo. Cottonwood and juniper trees are sparsely scattered along tributaries and more thickly along trunk channel banks.

The Arroyo de los Pinos outlet joins the Rio Grande at a 90° junction angle, with a local channel slope of 1.2% (Table 1). Non-engineered spoil levees north and south of the channel were installed in the 1960s to protect an agricultural drainage ditch culvert that crosses under the arroyo 200 m upstream of the confluence. The Arroyo de la Parida planform has a junction angle of < 90° (~70°) with the Rio Grande, as measured on the upstream side of the confluence, and a local channel slope of 1.2% (Table 1). The Parida tributary mouth has been modified by the United States Bureau of Reclamation, with the outlet widened and the banks lowered and graded to be gently sloping to improve off-channel refuge habitat for the endangered silvery minnow. The Arroyo de las Cañas has a 1.5% local channel slope and splits into two branches near the confluence with the Rio Grande, creating a vegetated bar. The northern, upstream branch has a junction angle > 90° (~110°) with the trunk stream and < 90° (~55°) with the southern branch, both measured towards the upstream bank (Table 1). The Bureau of Reclamation has periodically attempted to block off the upstream branch using earth-moving equipment, as sediment deposition at that mouth encourages the trunk stream to meander into a flood control levee on the opposite bank. However, the non-engineered sediment barrier has been repeatedly eroded.

3 Methods

We studied the sedimentary characteristics and the temporally varying morphology of these three ephemeral confluents of the mid-Rio Grande close to Socorro, New Mexico, focusing on the tributaries *upstream of the confluence*. Tributary stage hydrographs

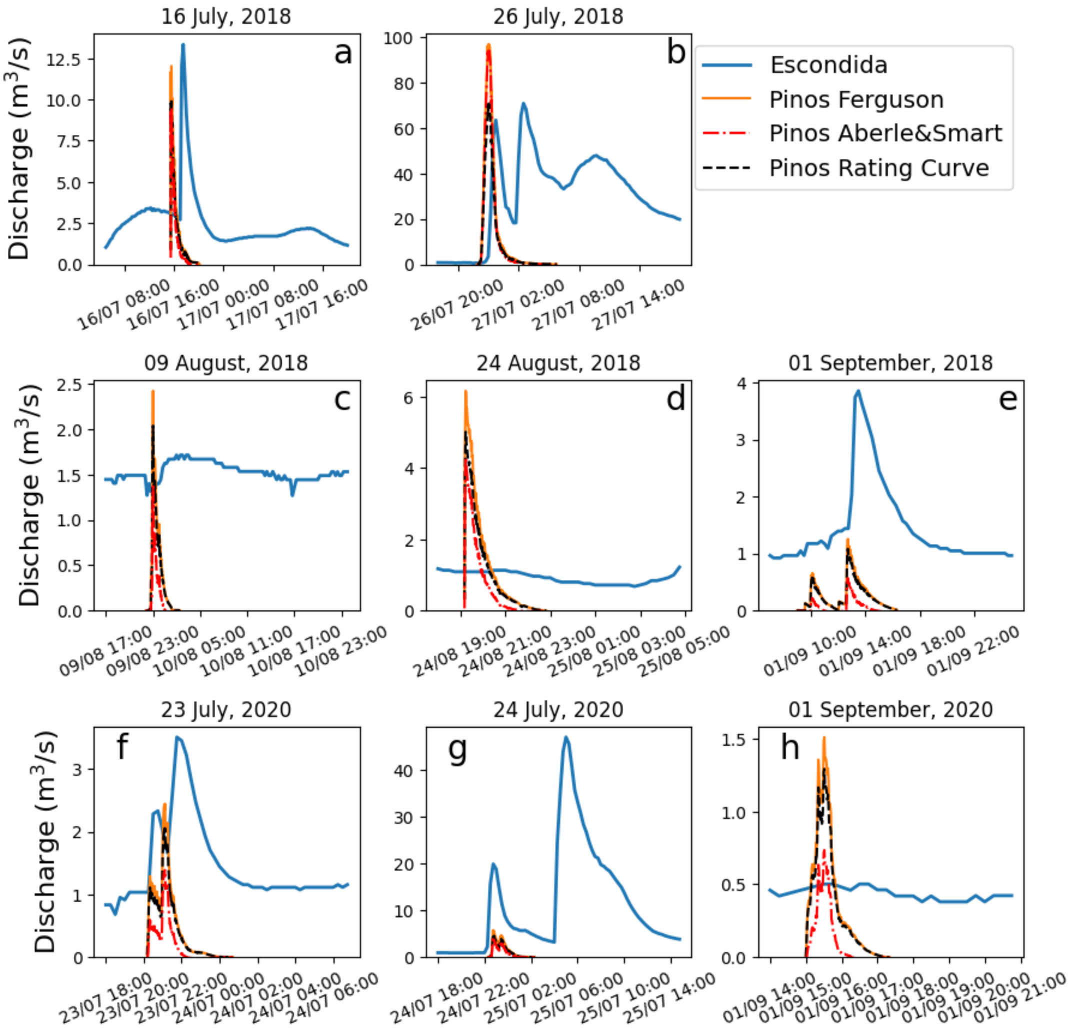

Figure 2 Discharge of the Arroyo de los Pinos and the Rio Grande at Escondida (3.5 km upstream of the junction) during flash flood events on the Pinos. Three methods of calculating the discharge of the Pinos from stage recordings are shown: the Manning-Strickler conversion of the 84th percentile bed material size (D_{84}) to Manning roughness coefficient (n) using the version from Ferguson (2007), a bed elevation standard deviation method to estimate the roughness parameter as proposed by Aberle and Smart (2003), and a local, fitted power-function stage-discharge rating curve developed from manually collected discharge measurements (Figure S4).

were calculated using pressure transducers at the Cañas and Parida outlets with a nearby barometric pressure transducer and a vented pressure transducer at the Arroyo de los Pinos. Data from stream gauges operated by the United States Geological Survey (USGS) were used to characterize the flow of trunk streams. Trenching the confluent deposits, we identified bedding type and thickness. Using repeat drone flights and applying Structure from Motion (SfM), we generated sequential orthophotographs and Digital Elevation Models (DEMs), from which we determined the temporally varying tributary morphology and estimated volumes of sediment storage from DEMs of Difference (DoD; Wheaton et al., 2010). A sensitivity study compared the three methods of change detection, choosing the optimal 95% confidence interval threshold for a Fuzzy Inference System. The methods are detailed hereafter.

3.1 Data Collection

Aerial photography for DEM construction was performed using a DJI Phantom 4 quadcopter drone paired with the smartphone application Pix4D to automate flight paths over the channels. The flights were flown at 30 m above ground level with an 80% photo overlap and a 90° camera angle from horizontal. For the Arroyo de la Parida, additional oblique photographs were flown at 15 m above ground level with an 80° camera angle in areas with steep banks. These 2.1 megapixel photos yielded 10-cm-pixel resolution DEMs. Aerial photography of all arroyos were conducted before and after the monsoon season. In the Arroyo de los Pinos, additional flights were conducted after major flow events. Ground control points were established to georeference the aerial imagery. Wooden 70 cm rectangular checkerboard markers were centered over permanent rebar monuments that were previously surveyed. Additionally, due to potential changes in ephemeral channel morphology, temporary rectangular 30 cm checkerboard markers were placed in the channels and surveyed using a Topcon IS robotic total station prior to each flight.

3.2 Structure from motion

Once aerial imagery was captured, SfM processing was undertaken using Metashape Professional (Agisoft LLC,

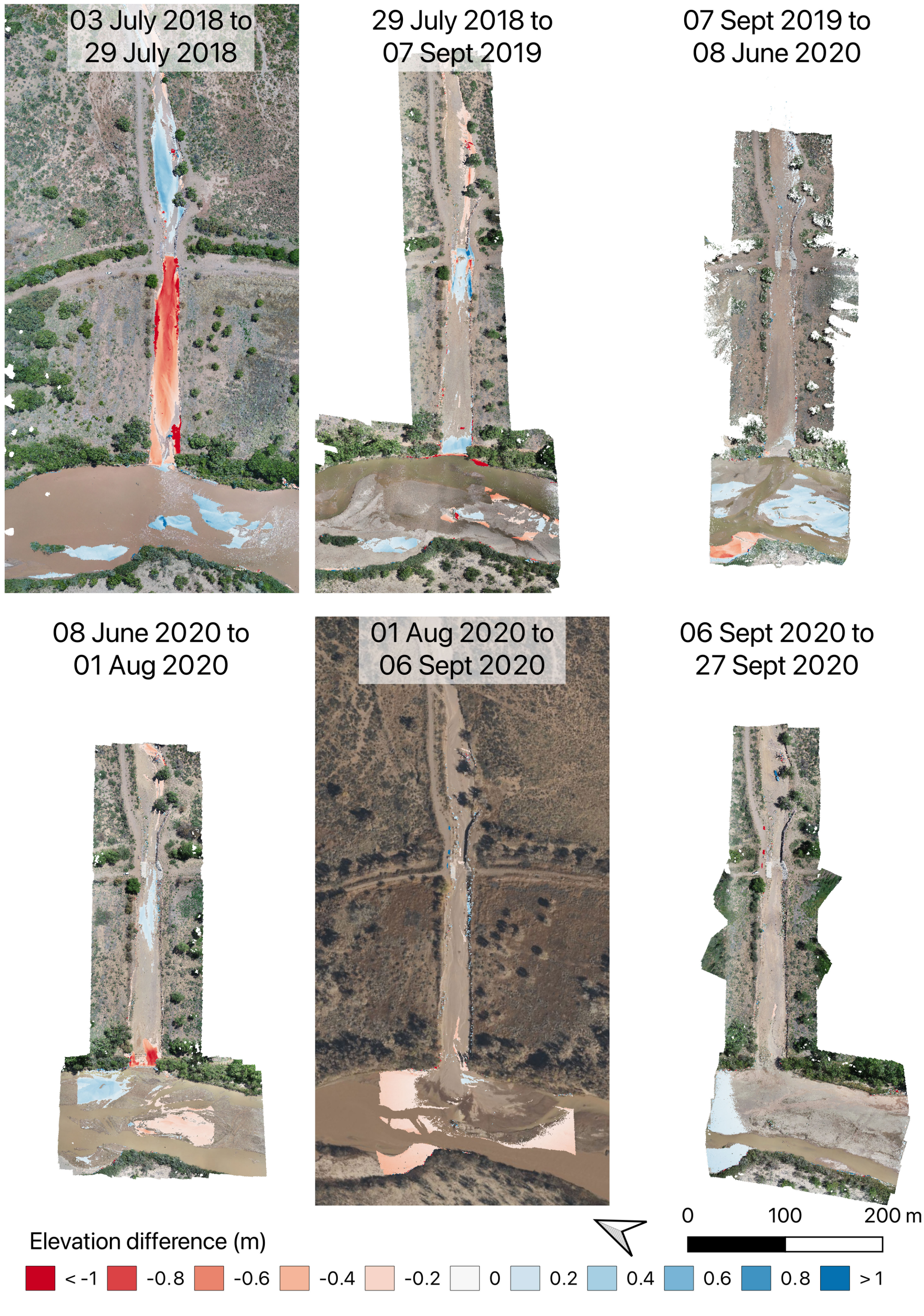

Figure 3 Six Digital Elevation Models (DEMs) of Difference (DoD) produced of the Arroyo de los Pinos junction. The detection threshold for change was estimated to be 0.1 m because the elevation root mean square error of checkpoints in the Structure from Motion derived point clouds was 0.05 m on average (minimum 0.01 m, maximum 0.09 m). The error was doubled to account for the error in both point clouds being differenced. Change values between -0.1 and 0.1 (i.e., below the threshold) are transparent in these images.

2020). This software creates three-dimensional renderings by constructing sparse point clouds, dense point clouds, DEMs, and orthophotos from the overlapping aerial photography. A post-processing workflow, created by the USGS and National Unmanned Aerial Systems Project Office (USGS National UAS Project Office, 2017), was used to eliminate inaccurate points that could warp the point cloud. User specified key points were used with a Scale Invariant Feature Transform algorithm to develop a sparse cloud of tie points and refine the camera locations.

Association of the checkerboard targets in the imagery with their surveyed coordinates enabled georeferencing and calculation of the accuracy of the point

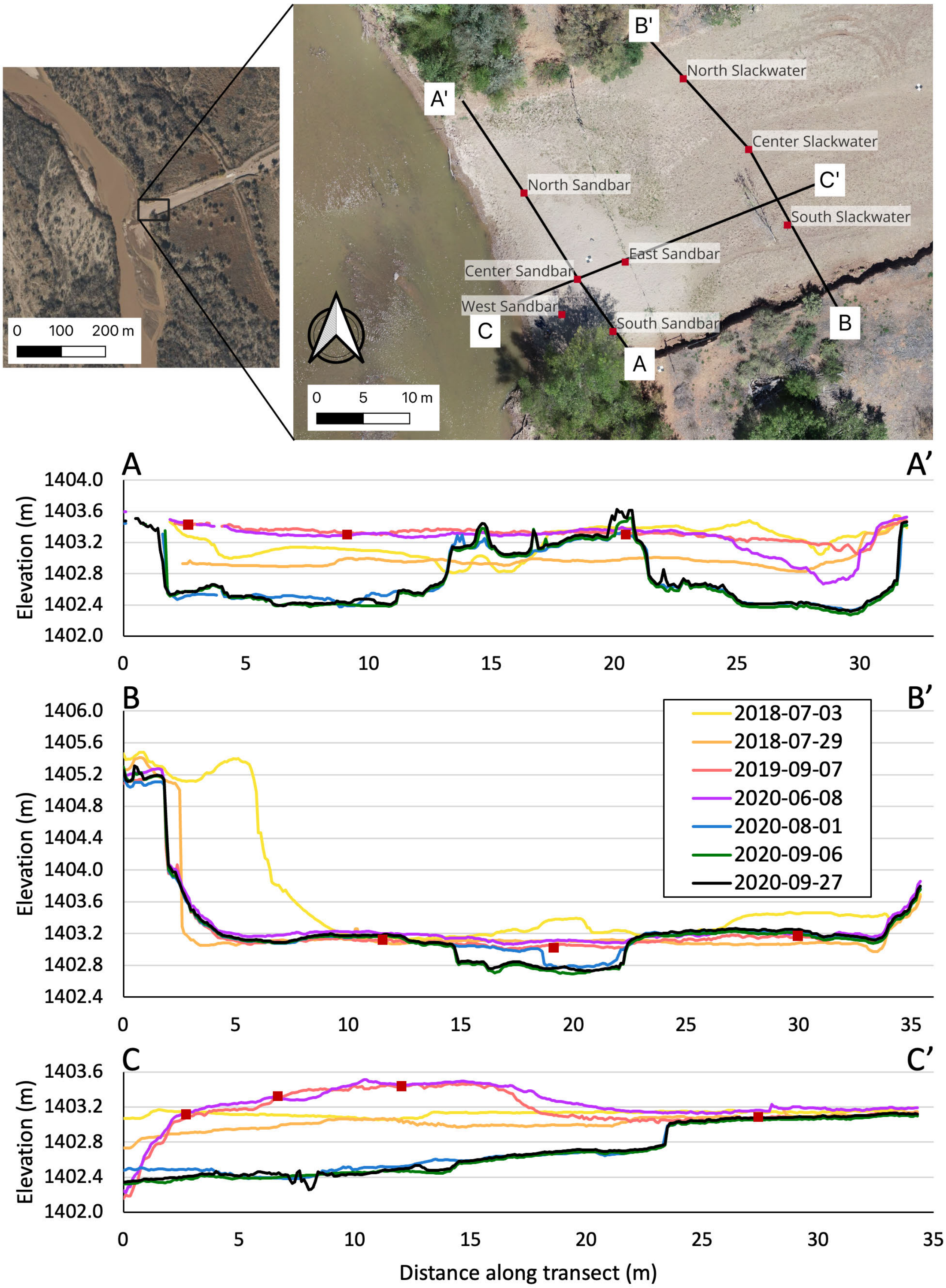

Figure 4 Aerial photographs and cross sections of the Arroyo de los Pinos outlet. The locations of the trenched pits are indicated by red squares on the maps and cross sections. Transect elevation profiles are extracted from Digital Elevation Models produced using Structure from Motion.

cloud elevations. Each flight used 20 – 24 surveyed control points, with roughly two thirds of the targets used as ground control points for active georeferencing of the point cloud. One third of the targets were used as checkpoints for the point cloud accuracy. The elevation root mean square error (RMSE) was calculated for both groups to quantify point cloud elevation accuracy (Wheaton et al., 2010; Cucchiaro et al., 2018). During dense point cloud processing in the Agisoft software, we selected ultra-high quality and mild depth filtering parameters to remove outliers resulting from poor image texture. Water surfaces were removed from the DEM processing due to challenges caused by specular reflection from ripples.

To evaluate changes in elevation between flow events, the DEM rasters were constructed and exported with concurrent grid sizes and spatial extents (Bailey, 2013). The Geomorphic Change Detection (GCD) software (Wheaton et al., 2010) was applied to compare the DEMs and compute a DoD, where positive DoD values indicate deposition and negative values indicate erosion. The GCD software offers a range of analyses to evaluate uncertainties present in the DEM rasters and identify significant topographic changes. A sensitivity study was conducted to determine the best method to extract a DoD among the following: (i) simple minimum level of detection, (ii) propagated errors, and (iii) probability analysis. The methods are fully explained in Wheaton et al. (2010). We determined that a simple minimum level of detection, with the detection threshold being the sum of the average RMSEs of the surveyed checkpoints for both flights being differenced, was optimal for assessing geomorphic change.

3.3 Water depth and discharge

Vented logging pressure transducers (SEBA DS-22) were installed at the Pinos sediment monitoring station, and unvented pressure transducers (Hobo U20) were emplaced in the Parida and Cañas tributaries in metal stilling wells to monitor flow events. Barometric pressure was also monitored to correct for changes in atmospheric pressure.

To convert the hydrostatic depth to discharge at the Arroyo de los Pinos, a local stage-discharge relationship (a rating curve) was constructed using manual cross-section average flow measurements (Table S1) and large-scale particle image velocimetry (LSPIV) surface velocities converted to discharge using the methods of Le Coz et al. (2021). One of the assumptions in this method is that the ratio ( ) of depth-averaged velocity to surface velocity is 0.85. We extrapolated discharge estimates to higher stages using a power function (Figure S1), which fit the data with an R-squared value (R^2) greater than 0.95.

We evaluated two other methods against this calibrated relationship, both of which use the Manning Equation,

$$Q = \frac{A(R_h^{2/3} S^{1/2})}{n}, \tag{1}$$

to estimate water discharge (Q), where A is cross-sectional area of flow calculated using a channel cross section survey and the water depth, R_h is the hydraulic radius calculated by dividing A by the wetted perimeter (P), which is also measured in the cross-section survey, S is the energy slope, which we estimated from a longitudinal bed slope survey extending over 100 m above and below the cross section, and n is a roughness coefficient.

The first alternative method estimates the roughness coefficient n using the Manning-Strickler relationship, which relates a roughness height scale, in our case, the 84$^{\text{th}}$ percentile bed material grain size (D_{84}), to n. We used the version of the relationship fitted by Ferguson (2007), which is equivalent to

$$n = \frac{D_{84}^{1/6}}{7.5 g^{1/2}} \tag{2}$$

where g is gravitational acceleration. The second alternative method estimates the roughness coefficient n using an empirical fit with the standard deviation of the detrended local bed elevation (σ) first reported by Aberle and Smart (2003) and subsequently tested using high resolution data similar to our SfM output (Brasington et al., 2012; Rychkov et al., 2012). This equation is equivalent to

$$n = \frac{R_h^{1/6}}{g^{1/2}\left(3.86 \ln\left(\frac{h}{\sigma}\right) - 1.19\right)} \tag{3}$$

where h is the depth of the water. We tested these alternative methods for reliability in our study area because we did not have calibrated rating curves at either of the Parida or Cañas arroyos.

For the Arroyo de la Parida, we converted the stage data to discharge using both of the alternative methods (i.e., Aberle and Smart, 2003; Ferguson, 2007), which was possible due to the drone-derived, high-resolution DEM at the gauging cross section. In the Arroyo de las Cañas, the pressure transducer was installed 1 km upstream from the photographed area, which was the nearest well-confined reach. Hence, a standard deviation of the DEM was not available. Instead, in addition to Ferguson's Manning-Strickler estimate of n based on a pebble count, we considered a third method, the empirical equation of Jarrett (1984), to estimate n for steep channels:

$$n = 0.39 S^{0.38} R_h^{-0.16}. \tag{4}$$

This equation was developed for steep, gravel-to-boulder bed channels in Colorado and is based on a statistical regression. Because it is a regression fit that does not attempt to separate different sources of friction, it likely incorporates some influence from energy dissipation processes beyond grain size, such as the formation of hydraulic jumps that are common in these steep channels at high flows. The bed material size of the Cañas is small compared to most of the training data of Jarrett (1984), but the channel is sufficiently steep. So, we considered it to calculate a maximum plausible n for these flow events (leading to a minimum discharge estimate). A comparison of the various roughness coefficient n estimates is provided in Table S2.

The Rio Grande water discharge was gauged by the USGS at Escondida Bridge (USGS Site ID: 08355050), located between our study tributaries. The Escondida Bridge gauge is 0.5 km downstream from the Arroyo de la Parida outlet, 3.5 km upstream from the Pinos, and 13 km upstream from the Cañas (Figure 1). Two other nearby USGS gauges on the Rio Grande were not used due to data gaps.

3.4 Trenching and stratification

Manual sediment sampling took place at the mouth of two of the arroyos, the Parida and Pinos, to characterize bed morphology and sedimentary character. Sedimentary structures can provide insight into the flow regime, energy, and direction. We photographed the trenched pits in the Parida and Pinos and marked each stratigraphic horizon. The Cañas was not trenched due to a tributary flow event that re-mobilized the mouth

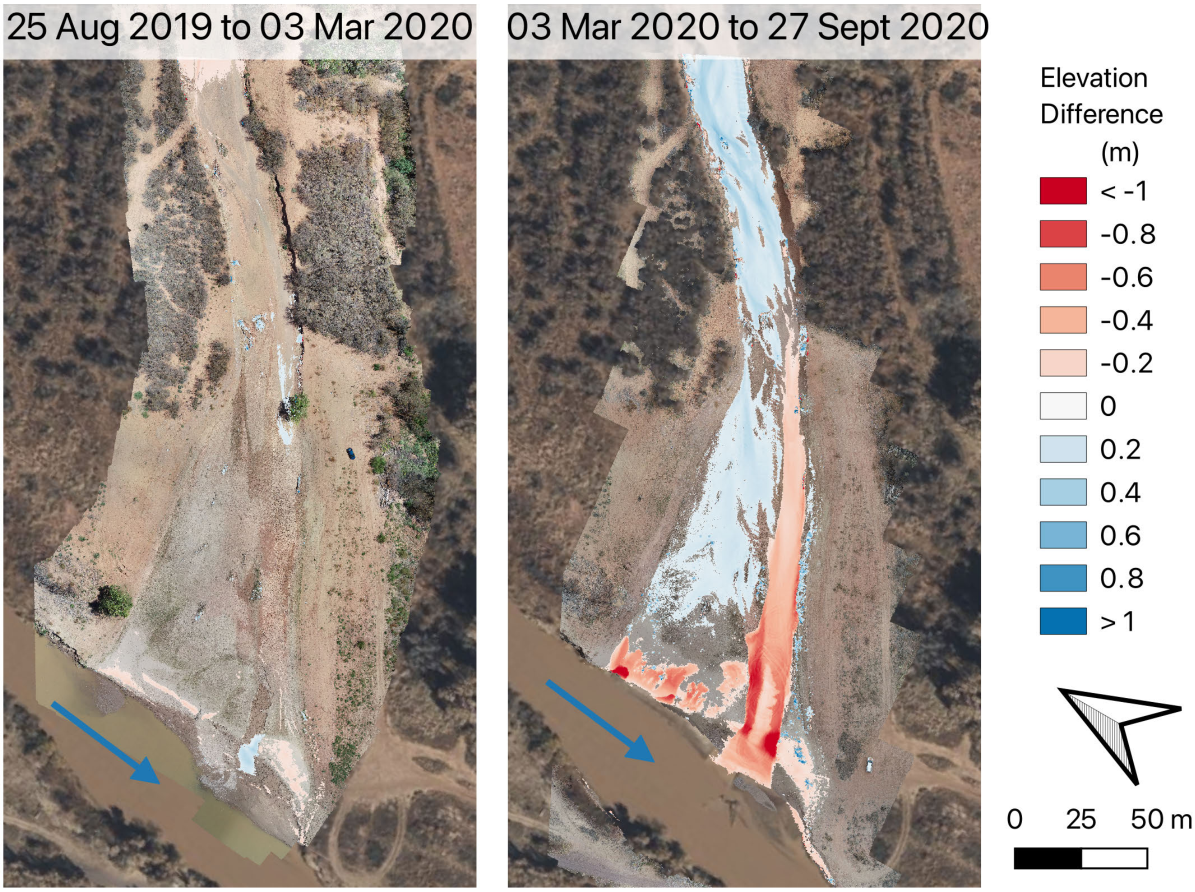

Figure 5 Two Digital Elevation Models (DEMs) of Difference (DoD) produced for the Arroyo de la Parida. Blue arrows indicate flow direction in the Rio Grande. The detection threshold for elevation changes was estimated to be 0.1 m, based on the root mean square error of point cloud checkpoints. Change values between -0.1 and 0.1 (i.e., below the threshold) are transparent in these images.

bars that had been deposited at both the southern and northern branches of the tributary junction before they could be sampled. Instead, photographs of the exposed facies were taken where the breaching of the bar had occurred.

Grain size for each stratigraphic horizon in the trenched pits was quantified. The trenched pits were dug down to a coarse gravel layer (transported by the tributary confluent), which was not sampled. The samples were analyzed first using 0.0625 – 2 mm sieves, and with a soil hydrometer 152H and a settling column to estimate ≤ 0.0625 mm size fractions using the method ASTM D7928. This technique requires an introduced mass of 50 g of sediment into the column, so we conducted hydrometer analyses only for samples with ≥ 50 g of fines, which was equivalent to about 10% of the mass of our samples from individual sedimentary layers. The sediment was dispersed with sodium hexametaphosphate. We collected hydrometer measurements beginning at 40 s for coarse silts, and extending to 24 hr for clays (nominally, 1 µm).

4 Results

4.1 Water discharge and topographic change

The relative discharge in the Rio Grande, compared to that of the three tributaries, was highly variable. Because the tributaries are ephemeral, usually the Rio Grande was the only channel with water. At these times, the stage of the Rio Grande controlled interactions with the tributaries. During high stages, such as spring runoff in 2019 (Figure S2), backwaters extended upstream into the tributaries, as much as 100 m beyond the mouth of the Pinos, and 200 m beyond the mouth of the Parida. In contrast, there were extended periods during the late spring and summer of 2018 and 2020 when both the Rio Grande and the tributaries were dry. Summer is also the season of monsoon-driven flash flooding from the tributaries. Therefore, we will distinguish the geomorphic changes we mapped as being from either the winter (non-monsoon) season or summer (monsoon) season (Figure S2).

The most dramatic change in relative discharge occurred when the tributaries experienced flash floods. This occurred at times when there was flow in the Rio Grande, but also occasionally occurred when the Rio Grande was dry. Hence, flow conditions at the tributary junctions varied from 100% flow in the trunk stream to 100% flow in the tributary (e.g., Figure 2b). The character of the observed geomorphic change during any given interval between drone mapping flights correlates with the relative flow conditions on the tributary and the Rio Grande. For example, when the Pinos had a large discharge into an essentially dry Rio Grande on 26 July 2018 (Figure 2b), extensive tributary bed erosion up to 0.8 m deep was observed (Figure 3; 03 July – 29 July). At

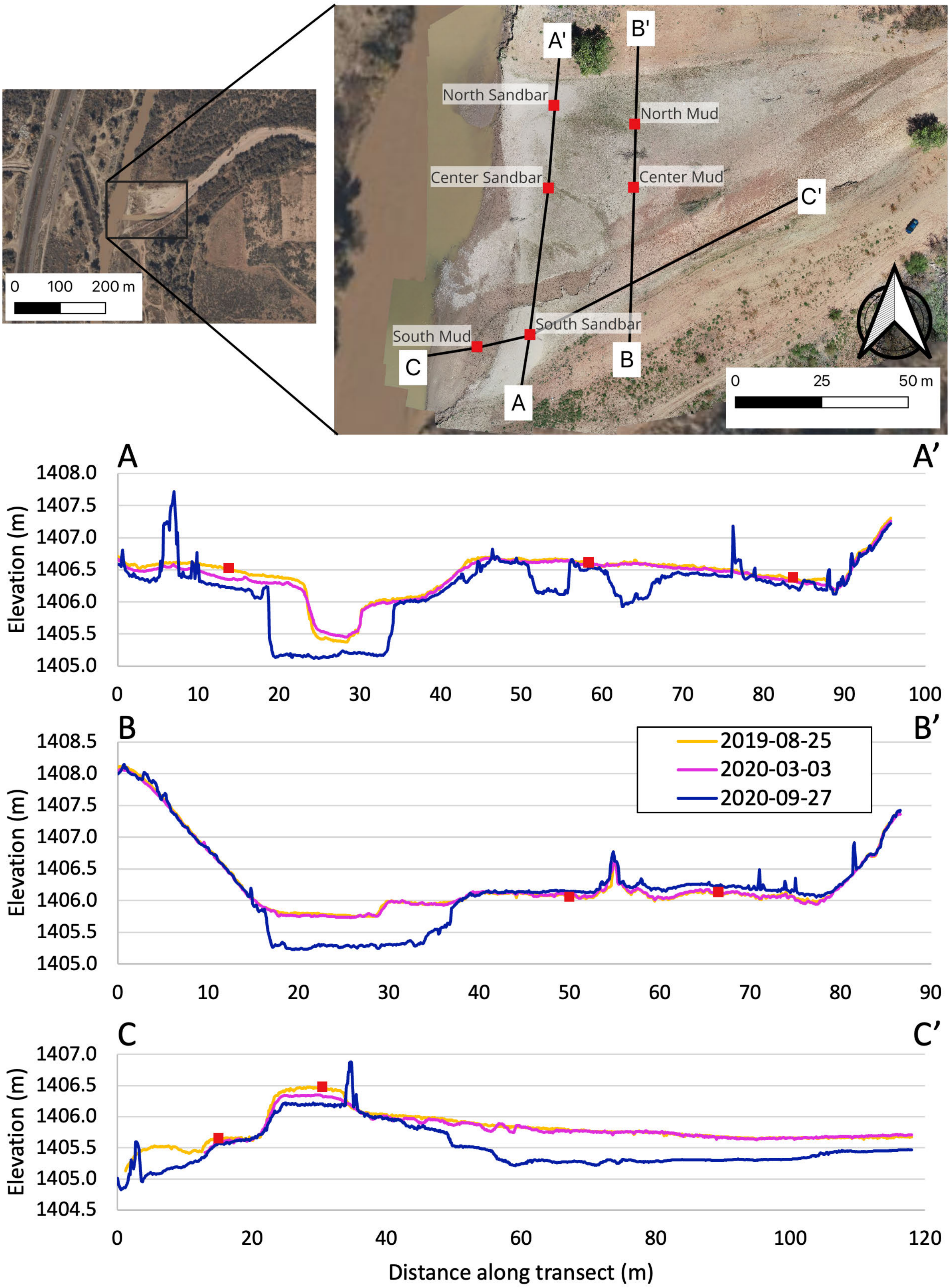

Figure 6 Aerial photographs and cross sections of the Arroyo de La Parida outlet. The locations of the trenched pits are indicated by red squares on the maps and cross sections. Transect elevations profiles are extracted from Digital Elevation Models produced using Structure from Motion.

the other extreme, during the extended high flows in the Rio Grande in spring 2019 (Figure S2), when there were no flash floods on the Pinos, a 0.5 – 0.7 m tall sand bar was deposited across the mouth of the Pinos (Figure 4). This bar was then partially dissected during a flash flood on 24 July 2020, lowering the channel bed in places by 1.0 m (Figures 3 and 4), when the Pinos delivered 5 m^3/s simultaneously with an increase of discharge on the Rio Grande to 20 m^3/s (Figure 2g). Hence, tributary incision does not require an absence of flow on the trunk stream, merely a greater transport capacity in the tributary and an adequately low stage in the trunk.

Topographic changes also occurred in these tributaries depending on their width, confluence angle, and

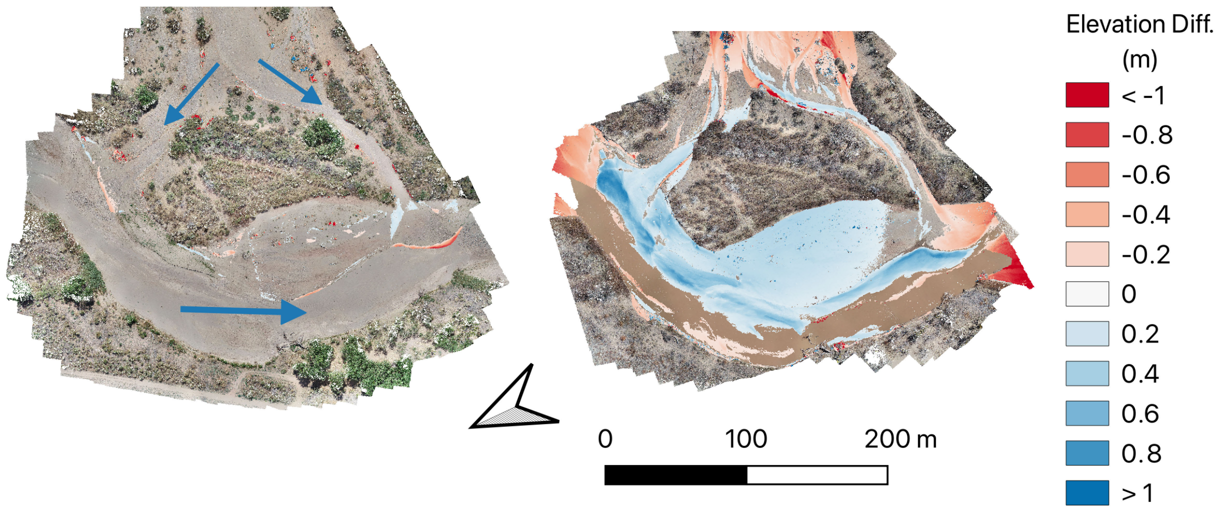

Figure 7 Two Digital Elevation Models (DEMs) of Difference (DoD) produced for the Arroyo de las Cañas. Blue arrows indicate flow direction. The detection threshold for elevation changes was estimated to be 0.1 m, based on the root mean square error of point cloud checkpoints. Change values between -0.1 and 0.1 (i.e., below the threshold) are transparent in these images.

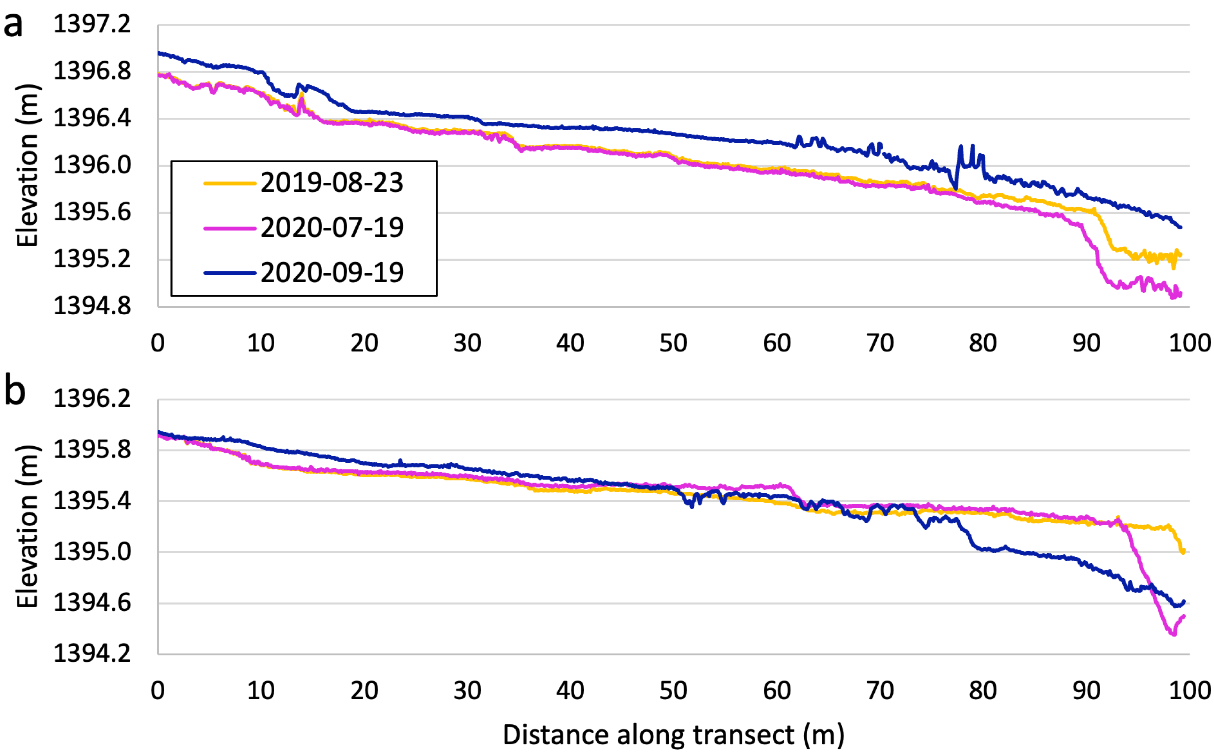

Figure 8 Longitudinal elevation profiles extracted from Digital Elevation Models at the Arroyo de las Cañas junction with the Rio Grande. The confluence has a northern upstream branch (**a**) and a southern downstream branch (**b**) visible in the map (Figure 7).

upstream stable section. The Arroyo de la Parida was widened at its confluence by the Bureau of Reclamation before this study to create an aquatic habitat. With this wide geometry, no topographic change was detected when small events occurred (Figure S3), but a flash flood on 24 July 2020 with a discharge of ~35 m^3/s caused deposition upstream within the channel and widening of a channel previously cut through the mouth bar (Figure 5). Deposition on the upstream side of the Parida confluence and erosion of the downstream side (Figure 6) were associated with the wider mouth and more acute junction angle of this confluence. In contrast, at the nearly 90° junction angle of the Pinos, extensive bar sedimentation occurred during Rio Grande high flows, especially on the downstream portion of the confluence (Figure 4, cross section C-C'). The Arroyo de las Cañas confluence comprises two outlets separated by a vegetated bar. Considerable (~1 m) deposition occurred in the northern, upstream outlet during a 14 m^3/s flash flood on 26 July 2020 (Figure S4). In contrast, half as much deposition and some localized erosion took place in the southern, downstream outlet (Figures 7 and 8), the latter having a smaller confluence angle with the Rio Grande, thereby facilitating the transfer of tributary sediment to the trunk river.

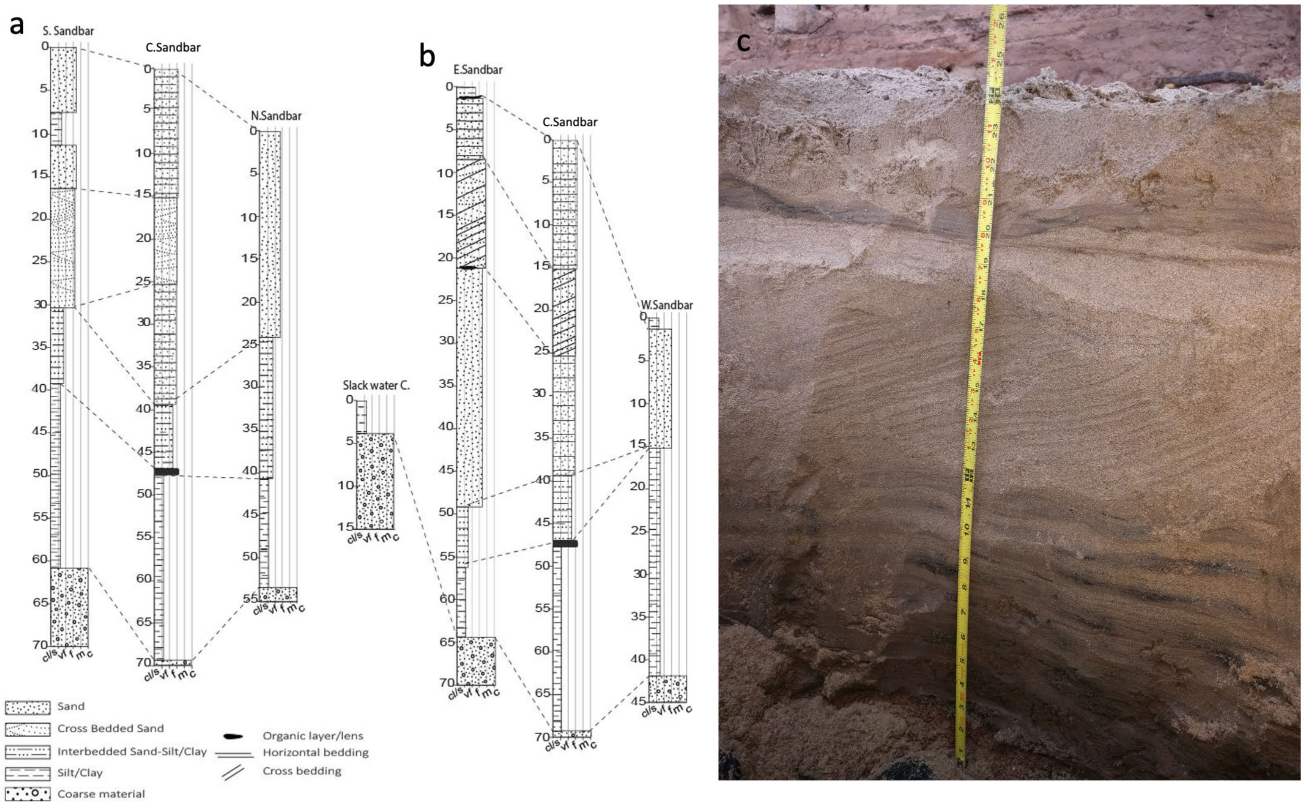

Figure 9 Stratigraphic columns and horizon interpretations for the pits dug at the Arroyo de los Pinos tributary junction (**a**) North-South transect A-A' (Figure 4) and (**b**) East-West transect C-C' (Figure 4). The columns are set to an internally consistent elevation datum. Grain size classes are clay/silt (cl/s), very fine sand (vf), fine sand (f), medium sand (m), and coarse sand (c). Photograph (**c**) of the south wall of the South Sandbar pit. Note the thick east-dipping cross beds, indicating eastward flow in the southern portion of the junction, consistent with clockwise circulation. The tape measure is marked in feet and inches. Additional photos are available in Supplemental Figure S5.

4.2 Sedimentary analysis

Further insights into the tributary junction dynamics can be gained by considering the stratigraphy of the mouth bar deposits at the Arroyo de los Pinos (Figure 9) and the Arroyo de la Parida (Figure 10). Both mouth bars formed during high Rio Grande flows (up to 125 m^3/s) in spring 2019 (Figure S2), which inundated the tributary mouths and formed backwaters. The sedimentary deposits in the Arroyo de los Pinos confluence (Figure S5) comprise lower clay layers overlain by fine sands and medium cross laminated sands, the latter overlain by slackwater and bank collapse clays (Figures 9a and 9c).

This succession is an indication that the Rio Grande's overbank deposition in the tributary mouth was generated by recirculatory flow (Picard and High, 1973). In this case, with the tributary on the river left, a clockwise pattern developed, with sedimentary deposits advancing eastward, up-tributary, from the southern, downstream, end of the tributary mouth (Figure S5a – d). A similar succession was laid in the Parida confluence, though the cross-stratification was much weaker, with less evidence of recirculatory flow. Yet there was still sandy gravel at the bottom of the sequence and as many as seven intercalations of clay laminae overlain by crossbedded sands (Figure 10). These may represent sequential deposition by slight changes in the generally increasing Rio Grande water levels during spring runoff (Figure S2). We also documented evidence of a small tributary flow event in July 2019 on the Parida cutting a narrow channel through the tributary mouth bar and dissecting a small fan (Figures 10c and 10d). This occurred prior to the installation of the stage gauge; therefore, we do not know the discharge.

5 Discussion

Having studied three small ephemeral tributaries of the mid-Rio Grande, we discuss the significance of the tributary areas located at and immediately upstream of their coalescence with a trunk stream. Four themes are covered: the relevance of the lowest reaches of ephemeral tributaries to (i) palaeohydrologic reconstructions, (ii) the geometry of junctions, (iii) hydraulic reconstruction, and (iv) their ecological significance.

5.1 Palaeohydrologic reconstructions

Slackwater deposits have been identified in a multitude of tributary settings, with the most common goal being to determine the discharge and age of trunk stream paleofloods (Patton and Schumm, 1981; Kochel and Baker, 1982; Baker et al., 2022), to a large extent with reference to channels in drylands (Ely and Baker, 1985; Greenbaum et al., 1998, 2000; Zituni et al., 2021). The stratigraphy of sediments deposited by very large floods often involves thick sequences (Benito et al., 2020). As stated in Carling (2013):

> *...Megaflood giant bar successions typically exhibit [variants on the following] sequence...from*

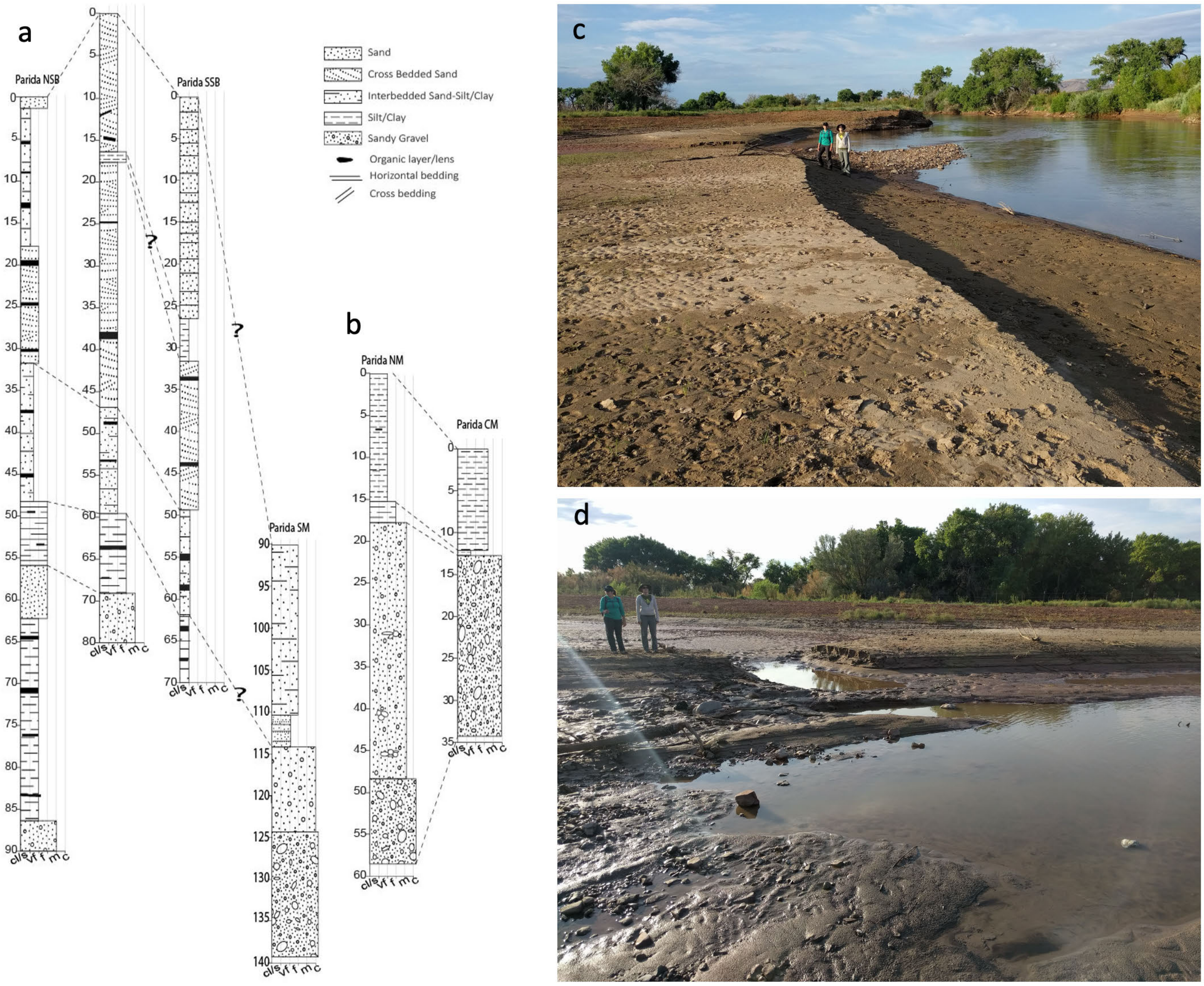

Figure 10 Stratigraphic columns and horizon interpretations for the pits dug (**a**) at the Arroyo de la Parida tributary junction western transect C-A' (Figure 6), including the north sandbar (NSB), center sandbar (CSB), south sandbar (SSB), and south mud (SM) sampling pits. Stratigraphic columns (**b**) eastern transect B-B' (Figure 6), including the north mud (NM) and center mud (CM) sampling pits. The columns are set to an internally consistent elevation datum, with the exception of the SM column, which has been translated upwards by ~40 cm depth to fit on the figure, with a depth numbering scheme consistent with the SSB pit. Grain size classes are clay/silt (cl/s), very fine sand (vf), fine sand (f), medium sand (m), and coarse sand (c). Photographs of the mouth bar on 22 July 2019, right after a small tributary flow event: (**c**) looking south along the bar crest (note the small gravel fan behind the people) taken from a position just west of the NSB pit location, before pits were dug, and (**d**) looking southeastward at the eroded breach in the mouth bar taken from the gravel fan.

> *the base to the top of each succession: (1) basal coarse parallel-bedded units; (2) large-scale [high-angle] clinoforms; (3) horizontally-bedded laminations; (4) ripple and dune cross-lamination; (5) silt beds and [in places,] (6) debris flow units. (pp. 93 – 94)*

Megaflood and ordinary flood deposits thin out as they back-flood upstream into tributaries from the main river (Benito and O'Connor, 2003). Recently, the description of slackwater deposits has also concerned identifying the transport of very large boulders (Greenbaum et al., 2020).

A recent treatise describes in detail the stratigraphy of slackwater deposits (Benito et al., 2023). However, none have mapped their spatial three-dimensional sedimentologic variability and their repeated partial-to-full destruction as we have after individual monitored flood events. The mouth bars preserve evidence of recirculatory flow, but this is dependent on the junction angle. And mouth bars may be partially (Figure 10d) or fully (Figure 3) eroded, depending on the relative size of the tributary flow event. We expect the duration of the temporary sediment sequestration to be on the order of 2 – 5 years.

5.2 The geometry of junctions

Stream junction angles depend on the local longitudinal slopes; hence, they typically decrease with a decrease in stream order, i.e., a decrease in stream size (Seybold et al., 2017; Strong and Mudd, 2022). We determined the junction angles between the studied tributaries and the trunk. The approximately right angles of the studied tributary junctions differ from and are larger than the acute angles common to the most widely studied perennial streams. We inventoried tributary junctions along the Rio Grande from Cochiti Dam near Santa Fe to Caballo Dam near Truth or Consequences, New Mexico, using aerial photography. Many tributaries have insufficient flow to maintain a channel through the riparian—mostly tamarisk—forests, and infiltrate. As the landscape is generally controlled by agricultural ditches, we excluded those tributaries that are held in place by levees, which dictate the junction angle. We identified 28 channel junctions into the Rio Grande, which include our three study channels. Their mean angle is ~83°, and the range is 43 – 107° (Figure S6).

The optimal angles of stream junctions are acute, often quite small (e.g., Howard, 1971), although as has recently been shown, they vary with climate, with an average of 45° in arid climates increasing to 72° in humid counterparts (Seybold et al., 2017). The Rio Grande tributary angles differ from the expected junction angles between channels of similar order, as quoted above, because they refer to very small tributaries having large longitudinal slopes of 1% or greater, entering a major artery with a bed slope of 0.07% (Strong and Mudd, 2022). This difference in slope likely has a major influence on tributary areas of erosion and deposition, thereby enabling the maintenance of right-angle junctions. It is also possible that the commonly deposited mouth bars and the direct incisions made by small floods as they breach them may contribute to the prevalence of 90° junction angles in ephemeral tributaries.

5.3 Hydraulic reconstruction

Few engineering studies describe design approaches regarding the lowermost reach of a tributary for practical purposes, such as depositional space or for ecological enhancement. There is a practical need for a cornerstone paper depicting the hydraulic design and characteristics of widened tributaries for the purpose of increased local heterogeneity and improved habitat diversity and connectivity. This has been demonstrated in both hydraulic models as well as in the Upper Rhine River (Leite Ribeiro et al., 2012b).

Studies such as ours can be useful to the engineering design of the confluence of ephemeral tributaries with trunk streams. The increased morphologic stability of the trunk stream, by means of the temporary storage of sediment in the tributary mouth, may be considered a beneficial service of ephemeral tributaries that could be enhanced by engineering designs. Such storage may alleviate aggradation and degradation by allowing large volumes of sediment deposited by a trunk stream to be mobilized by tributaries after the passage of trunk floods (Posner, 2021).

5.4 Ecological significance of upstream confluence areas

With few exceptions, the literature on tributary junctions has concentrated on the area below the junction and somewhat on the nearby upstream trunk area, inclusive of ecological effects (e.g., Benda et al., 2004b; Foulquier et al., 2024). Ours is a first attempt to evaluate the extent to which the morpho-texture of a tributary's area evolves temporally. We identify both small and large variations in bed elevation resulting from slackwater deposition and its erosion by tributary flows, which occur due to the lack of contemporaneity between trunk and tributary flows during flood events. This suggests that the temporary nature of bed height has ramifications for the ecology of these short upstream reaches that deserve further study. For instance, the import of organic matter and seeds may allow the growth of plants, provide ecosystem services, and maintain biodiversity (Vidal-Abarca Gutierrez et al., 2023).

The increased biologic resilience of widening lower tributaries is stressed by the following quotation:

> *The periodic reversal of sediment distribution that you describe may have ecological effects beyond just those on vegetation. There is a good chance it would alter hyporheic flow patterns, interstitial organic matter and fine materials, and microbial productivity—at least transiently—and these could, in turn, affect productivity and water quality at the surface (evidenced by transitional changes in benthic algae and diatoms in upwelling zones, for example). It may also affect nutrient dynamics in the receiving river. If surface sediment particle size is substantially altered, that may also affect benthic invertebrate habitats—again, transitionally. But these transitional changes are likely to enhance the biodiversity over time and contribute to system resilience (Andrew Boulton, personal communication, 2023).*

6 Conclusions

We have summarized the available, sparse information on the confluence of ephemeral channels. The outlet of ephemeral channels upstream of the trunk confluence is affected by trunk deposition of high concentrations of sediments, mainly sand bars. The tributaries transport large masses of sediment, inclusive of coarse gravel, thereby affecting the confluence of the trunk, at times depositing large bars. With increased distance above the trunk into the tributary confluent, the depth of trunk backwaters decreases, and thus bar texture fines upstream in the confluent. Bar thickness similarly fades upstream. The stratification of sand with some granules documents the circulatory flow in the lowermost tributary area. The tributary area above the confluence is at times scoured by flash floods, hence trunk deposits are preserved longer in protected areas located along confluent banks.

The tributary confluent areas upstream of the junction are the hot spots where trunk flood sediments are preserved. Unlike the characteristically small, acute angles between similarly sized tributaries, those between an ephemeral tributary and a much larger trunk are larger, typically approaching 90°. The resulting mouth bar geometry and recirculatory flow create depositional environments that provide a basis from which to consider the environmentally noteworthy conditions of these oft-neglected fluvial areas.

Acknowledgements

The authors gratefully acknowledge the thoughtful comments of two anonymous reviewers. We thank Kyle

Stark, Zachary Chavez, Madeline Richards, and Kelsey Romero for assistance with field work. Bill Holmes graciously provided land access. We thank Andrew Boulton for discussions increasing our awareness of environmental implications.

Land Recognition

This work was completed from an institution located on the ancestral lands of the Piro and Mescalero Apache peoples. We recognize and honor the land and the people who have stewarded it throughout the generations.

Data and Codes Availability

Digital elevation models are archived on Zenodo at DOI https://doi.org/10.5281/zenodo.15706974 under the title "Elevation data used to analyze non-contemporaneity of flow events in ephemeral tributary junctions". Tributary water discharge data for the Arroyo de los Pinos is archived and publicly available on the US Bureau of Reclamation "Reclamation Information Sharing Environment" (RISE) database (https://data.usbr.gov).

Funding Statement

This research was supported by the U.S. Bureau of Reclamation S&T program (project 9781: "Ephemeral tributary sediment transport measurement"). Additional student funding from the New Mexico Geological Society is gratefully acknowledged.

Conflict of Interest Disclosure

The authors declare that we have no competing or interests, financial or otherwise, related to this research.

Permission to Reproduce Material from Copyrighted Sources

The authors declare that no material from copyrighted sources was reproduced in this manuscript.

Declaration on Artificial Intelligence Use

The authors declare that no artificial intelligence tool was used to assist in or generate any part of the contents in this manuscript.

References

Aberle, J. and Smart, G. The influence of roughness structure on flow resistance on steep slopes. *Journal of hydraulic research*, 41(3):259–269, 2003. doi: 10.1080/00221680309499971.

Agisoft LLC. *Agisoft Metashape User Manual*, 2020, https://www.agisoft.com.

Ali, H. L., Yusuf, B., Mohammed, T. A., Shimizu, Y., Ab Razak, M. S., and Rehan, B. M. Improving the hydro-morpho dynamics of a river confluence by using vanes. *Resources*, 8(1):9, 2019. doi: 10.3390/resources8010009.

Ashmore, P. E. Laboratory modelling of gravel braided stream morphology. *Earth Surface Processes and Landforms*, 7(3):201–225, 1982. doi: 10.1002/esp.3290070301.

Azma, A. and Zhang, Y. The effect of variations of flow from tributary channel on the flow behavior in a T-shape confluence. *Processes*, 8(5):614, 2020. doi: 10.3390/pr8050614.

Bailey, P. Data Preparation - Best Practices, 2013, https://gcd.riverscapes.net/Concepts/data-preparation---best-practices/.

Baker, V. R. Paleoflood hydrology: Origin, progress, prospects. *Geomorphology*, 101(1-2):1–13, 2008. doi: 10.1016/j.geomorph.2008.05.016.

Baker, V. R., Kochel, R. C., Patton, P. C., and Pickup, G. Palaeohydrologic analysis of Holocene flood slack-water sediments. In *Modern and Ancient Fluvial Systems*, edited by Collinson, J. and Lewin, J., pages 229–239. John Wiley & Sons, Ltd., 1983. doi: 10.1002/9781444303773.ch18.

Baker, V. R., Benito, G., Brown, A. G., Carling, P. A., Enzel, Y., Greenbaum, N., Herget, J., Kale, V. S., Latrubesse, E. M., Macklin, M. G., et al. Fluvial palaeohydrology in the 21st century and beyond. *Earth Surface Processes and Landforms*, 47(1):58–81, 2022. doi: 10.1002/esp.5275.

Benda, L., Andras, K., Miller, D., and Bigelow, P. Confluence effects in rivers: interactions of basin scale, network geometry, and disturbance regimes. *Water Resources Research*, 40(5), 2004a. doi: 10.1029/2003WR002583.

Benda, L., Poff, N. L., Miller, D., Dunne, T., Reeves, G., Pess, G., and Pollock, M. The network dynamics hypothesis: how channel networks structure riverine habitats. *BioScience*, 54(5):413–427, 2004b. doi: 10.1641/0006-3568(2004)054[0413:TNDHHC]2.0.CO;2.

Benito, G. and O'Connor, J. E. Number and size of last-glacial Missoula floods in the Columbia River valley between the Pasco Basin, Washington, and Portland, Oregon. *Geological Society of America Bulletin*, 115(5):624–638, 2003. doi: 10.1130/0016-7606(2003)115<0624:NASOLM>2.0.CO;2.

Benito, G., Sánchez-Moya, Y., and Sopeña, A. Sedimentology of high-stage flood deposits of the Tagus River, Central Spain. *Sedimentary Geology*, 157(1-2):107–132, 2003. doi: 10.1016/S0037-0738(02)00196-3.

Benito, G., Harden, T., and O'Connor, J. Quantitative Paleoflood Hydrology. In *Treatise on Geomorphology*, edited by Schroder, J., volume 6.2, pages 743–764. Academic Press, 2nd edition, 2020. doi: 10.1016/B978-0-12-409548-9.12495-9.

Benito, G., Ballesteros-Cánovas, J., and Díez-Herrero, A. Paleoflood hydrology: reconstructing rare events and extreme flood discharges. In *Paleoflood Hydrology - Hydro-Meteorological Hazards, Risks, and Disasters*, edited by Shroder, J. F., Paron, P., and Di Baldassarre, G., pages 33–83. Elsevier, 2nd edition, 2023. doi: 10.1016/B978-0-12-819101-9.00009-1.

Best, J. and Rhoads, B. Sediment transport, bed morphology and the sedimentology of river channel confluences. In *River Confluences, Tributaries and the Fluvial Network*, edited by Rice, S., Roy, A., and Rhoads, B., pages 45–72. John Wiley & Sons, Ltd., 2008. doi: 10.1002/9780470760383.ch4.

Best, J. L. Sediment transport and bed morphology at river channel confluences. *Sedimentology*, 35(3):481–498, 1988. doi: 10.1111/j.1365-3091.1988.tb00999.x.

Best, J. L. and Reid, I. Separation zone at open-channel junctions. *Journal of Hydraulic Engineering*, 110(11):1588–1594, 1984. doi: 10.1061/(ASCE)0733-9429(1984)110:11(1588).

Biron, P., Roy, A., Best, J. L., and Boyer, C. J. Bed morphology and sedimentology at the confluence of unequal depth channels. *Geomorphology*, 8(2-3):115–129, 1993. doi: 10.1016/0169-

555X(93)90032-W.

Bombar, G. and Cardoso, A. Effect of the sediment discharge on the equilibrium bed morphology of movable bed open-channel confluences. *Geomorphology*, 367:107329, 2020. doi: 10.1016/j.geomorph.2020.107329.

Bourke, M. and Pickup, J. Fluvial form variability in Central Australia. In *Varieties of Fluvial Form*, edited by Miller, A. and Gupta, A., pages 249–271. Wiley, 1999.

Boyer, C., Roy, A. G., and Best, J. L. Dynamics of a river channel confluence with discordant beds: Flow turbulence, bed load sediment transport, and bed morphology. *Journal of Geophysical Research: Earth Surface*, 111(F4), 2006. doi: 10.1029/2005JF000458.

Bradbrook, K., Lane, S., and Richards, K. Numerical simulation of three-dimensional, time-averaged flow structure at river channel confluences. *Water Resources Research*, 36(9):2731–2746, 2000. doi: 10.1029/2000WR900011.

Brasington, J., Vericat, D., and Rychkov, I. Modeling river bed morphology, roughness, and surface sedimentology using high resolution terrestrial laser scanning. *Water Resources Research*, 48 (11), 2012. doi: 10.1029/2012WR012223.

Canelas, O. B., Ferreira, R. M., and Cardoso, A. H. Hydromorphodynamics of an open-channel confluence with bed discordance at dynamic equilibrium. *Water Resources Research*, 58 (1):e2021WR029631, 2022. doi: 10.1029/2021WR029631.

Carling, P. A. Freshwater megaflood sedimentation: What can we learn about generic processes? *Earth-Science Reviews*, 125: 87–113, 2013. doi: 10.1016/j.earscirev.2013.06.002.

Cucchiaro, S., Maset, E., Fusiello, A., Cazorzi, F., et al. 4D-SfM photogrammetry for monitoring sediment dynamics in a debris-flow catchment: software testing and results comparison. *International Archives of the Photogrammetry, Remote Sensing and Spatial Information Sciences*, 42(2):281–288, 2018. doi: 10.5194/isprs-archives-XLII-2-281-2018.

Dixon, S. J., Smith, G. H. S., Best, J. L., Nicholas, A. P., Bull, J. M., Vardy, M. E., Sarker, M. H., and Goodbred, S. The planform mobility of river channel confluences: Insights from analysis of remotely sensed imagery. *Earth-Science Reviews*, 176:1–18, 2018. doi: 10.1016/j.earscirev.2017.09.009.

Duguay, J., Biron, P., and Lacey, J. Aerial observations and numerical simulations confirm density-driven streamwise vortices at a river confluence. *Water Resources Research*, 58(7): e2021WR031527, 2022. doi: 10.1029/2021WR031527.

Ely, L. L. and Baker, V. R. Reconstructing paleoflood hydrology with slackwater deposits: Verde River, Arizona. *Physical Geography*, 6(2):103–126, 1985. doi: 10.1080/02723646.1985.10642266.

Ferguson, R. Flow resistance equations for gravel-and boulder-bed streams. *Water Resources Research*, 43(5), 2007. doi: 10.1029/2006WR005422.

Foulquier, A., Datry, T., Corti, R., Von Schiller, D., Tockner, K., Stubbington, R., Gessner, M. O., Boyer, F., Ohlmann, M., Thuiller, W., et al. Unravelling large-scale patterns and drivers of biodiversity in dry rivers. *Nature Communications*, 15(1):7233, 2024. doi: 10.1038/s41467-024-50873-1.

Ghobadian, R. Prediction of progressive penetration of scour hole into the tributary channel in laboratory channel confluences. *Journal of Applied Sciences*, 12(3):289–295, 2012. doi: 10.3923/jas.2012.289.295.

Greenbaum, N., Margalit, A., Schick, A. P., Sharon, D., and Baker, V. R. A high magnitude storm and flood in a hyperarid catchment, Nahal Zin, Negev Desert, Israel. *Hydrological Processes*, 12(1):1–23, 1998. doi: 10.1002/(SICI)1099-1085(199801)12:1<1::AID-HYP559>3.0.CO;2-6.

Greenbaum, N., Schick, A. P., and Baker, V. R. The palaeoflood record of a hyperarid catchment, Nahal Zin, Negev Desert, Israel. *Earth Surface Processes and Landforms*, 25(9): 951–971, 2000. doi: 10.1002/1096-9837(200008)25:9<951::AID-ESP110>3.0.CO;2-8.

Greenbaum, N., Schwartz, U., Carling, P., Bergman, N., Mushkin, A., Zituni, R., Halevi, R., Benito, G., and Porat, N. Frequency of boulders transport during large floods in hyperarid areas using paleoflood analysis–an example from the Negev Desert, Israel. *Earth-Science Reviews*, 202:103086, 2020. doi: 10.1016/j.earscirev.2020.103086.

Howard, A. D. Optimal angles of stream junction: Geometric, stability to capture, and minimum power criteria. *Water Resources Research*, 7(4):863–873, 1971. doi: 10.1029/WR007i004p00863.

Jarrett, R. D. Hydraulics of high-gradient streams. *Journal of Hydraulic Engineering*, 110(11):1519–1539, 1984. doi: 10.1061/(ASCE)0733-9429(1984)110%3A11(1519).

Kochel, R. C. and Baker, V. R. Paleoflood hydrology. *Science*, 215 (4531):353–361, 1982. doi: 10.1126/science.215.4531.353.

Le Coz, J., Renard, B., Vansuyt, V., Jodeau, M., and Hauet, A. Estimating the uncertainty of video-based flow velocity and discharge measurements due to the conversion of field to image coordinates. *Hydrological Processes*, 35(5):e14169, 2021. doi: 10.1002/hyp.14169.

Leite Ribeiro, M. *Influence of tributary widening on confluence morphodynamics*. PhD thesis, École Polytechnique Fédérale de Lausanne, 2011, https://infoscience.epfl.ch/record/169900.

Leite Ribeiro, M., Blanckaert, K., Roy, A., and Schleiss, A. Flow and sediment dynamics in channel confluences. *Journal of Geophysical Research: Earth Surface*, 117(F1), 2012a. doi: 10.1029/2011JF002171.

Leite Ribeiro, M., Blanckaert, K., Roy, A., and Schleiss, A. Hydromorphological implications of local tributary widening for river rehabilitation. *Water Resources Research*, 48(10), 2012b. doi: 10.1029/2011WR011296.

Liu, T., Fan, B., and Lu, J. Sediment–flow interactions at channel confluences: a flume study. *Advances in Mechanical Engineering*, 7(6):1–9, 2015. doi: 10.1177/1687814015590525.

McKee, E. D. Original structures in Colorado River flood deposits of Grand Canyon. *Journal of Sedimentary Research*, 8(3):77–83, 1938. doi: 10.1306/d4269003-2b26-11d7-8648000102c1865d.

Miller, J. P. High mountain streams: effects of geology on channel characteristics and bed material. Memoir 4, State Bureau of Mines and Mineral Resources, New Mexico Inst. of Mining and Technology, 1958.

Milner, V. S., Yarnell, S. M., and Peek, R. A. The ecological importance of unregulated tributaries to macroinvertebrate diversity and community composition in a regulated river. *Hydrobiologia*, 829(1):291–305, 2019. doi: 10.1007/s10750-018-3840-4.

Mosley, M. P. An experimental study of channel confluences. *The Journal of Geology*, 84(5):535–562, 1976. doi: 10.1086/628230.

Patton, P. C. and Schumm, S. A. Ephemeral-stream processes: implications for studies of Quaternary valley fills. *Quaternary Research*, 15(1):24–43, 1981. doi: 10.1016/0033-5894(81)90112-5.

Pelletier, J. D., Hayes, R. G., Hoch, O., Fenerty, B., and McGuire, L. A. Geometric constraints on tributary fluvial network junction angles. *Earth Surface Dynamics*, 13(2):219–238, 2025. doi: 10.5194/esurf-13-219-2025.

Picard, M. D. and High, L. R. *Sedimentary Structures of Ephemeral Streams*, volume 17 of *Developments in Sedimentology*. Elsevier, 1973.

Posner, A. J. Habitat Improvement within Escondida burn area monitoring Report, Middle Rio Grande Project, New Mexico.

Technical report, U.S. Bureau of Reclamation, Upper Colorado Basin Region, Albuquerque Area Office, Technical Services Division, 2021.

Reid, I. and Frostick, L. E. Channel form, flows and sediments of endogenous ephemeral rivers in deserts. In *Arid Zone Geomorphology*, edited by Thomas, D. S. G. John Wiley & Sons, 2011. doi: 10.1002/9780470710777.ch13.

Reid, I., Best, J., and Frostick, L. E. Floods and flood sediments in river confluences. In *Floods: Hydrological, Sedimentological and Geomorphological Implications*, edited by Beven, K. and Carling, P., chapter 8. John Wiley & Sons, 1989.

Rhoads, B. L. The dynamics of river confluences. In *River Dynamics: Geomorphology to Support Management*, edited by Rhoads, B. L., chapter 12. Cambridge University Press, 2020. doi: 10.1017/9781108164108.

Rhoads, B. L. and Sukhodolov, A. N. Spatial and temporal structure of shear layer turbulence at a stream confluence. *Water Resources Research*, 40(6), 2004. doi: 10.1029/2003WR002811.

Rhoads, B. L., Riley, J. D., and Mayer, D. R. Response of bed morphology and bed material texture to hydrological conditions at an asymmetrical stream confluence. *Geomorphology*, 109(3-4): 161–173, 2009. doi: 10.1016/j.geomorph.2009.02.029.

Rice, S. P., Kiffney, P., Greene, C., and Pess, G. R. The ecological importance of tributaries and confluences. In *River Confluences, Tributaries and the Fluvial Network*, edited by Rice, S. P., Roy, A. G., and Rhoads, B. L. John Wiley & Sons, 2008. doi: 10.1002/9780470760383.ch11.

Rychkov, I., Brasington, J., and Vericat, D. Computational and methodological aspects of terrestrial surface analysis based on point clouds. *Computers & Geosciences*, 42:64–70, 2012. doi: 10.1016/j.cageo.2012.02.011.

Sabrina, S., Lewis, Q., and Rhoads, B. Large-scale particle image velocimetry reveals pulsing of incoming flow at a stream confluence. *Water Resources Research*, 57(9):e2021WR029662, 2021. doi: 10.1029/2021WR029662.

Schindfessel, L., Creëlle, S., and De Mulder, T. How different cross-sectional shapes influence the separation zone of an open-channel confluence. *Journal of Hydraulic Engineering*, 143(9): 04017036, 2017. doi: 10.1061/(ASCE)HY.1943-7900.0001336.

Schumm, S. A. Effect of sediment characteristics on erosion and deposition in ephemeral-stream channels. Technical Report 352-C, U.S. Geological Survey, 1961.

Seybold, H., Rothman, D. H., and Kirchner, J. W. Climate's watermark in the geometry of stream networks. *Geophysical Research Letters*, 44(5):2272–2280, 2017. doi: 10.1002/2016GL072089.

Stark, K., Cadol, D., Varyu, D., and Laronne, J. B. Direct, continuous measurements of ultra-high sediment fluxes in a sandy gravel-bed ephemeral river. *Geomorphology*, 382:107682, 2021. doi: 10.1016/j.geomorph.2021.107682.

Stark, K., Cadol, D., Leary, K., and Laronne, J. B. Persistently high bedload flux in ephemeral channels. *Geomorphica*, 1(1), 2024. doi: 10.59236/geomorphica.v1i1.38.

Stokes, M. and Mather, A. E. Controls on modern tributary-junction alluvial fan occurrence and morphology: High Atlas Mountains, Morocco. *Geomorphology*, 248:344–362, 2015. doi: 10.1016/j.geomorph.2015.08.003.

Strong, C. M. and Mudd, S. M. Explaining the climate sensitivity of junction geometry in global river networks. *Proceedings of the National Academy of Sciences*, 119(50):e2211942119, 2022. doi: 10.1073/pnas.2211942119.

Sukhodolov, A. N., Krick, J., Sukhodolova, T. A., Cheng, Z., Rhoads, B. L., and Constantinescu, G. S. Turbulent flow structure at a discordant river confluence: Asymmetric jet dynamics with implications for channel morphology. *Journal of Geophysical Research: Earth Surface*, 122(6):1278–1293, 2017. doi: 10.1002/2016JF004126.

Swanson, B. J. and Meyer, G. Tributary confluences and discontinuities in channel form and sediment texture: Rio Chama, NM. *Earth Surface Processes and Landforms*, 39(14):1927–1943, 2014. doi: 10.1002/esp.3586.

Thornes, J. B. Channel processes, evolution, and history. In *Geomorphology of Desert Environments*, edited by Abrahams, A. and Parsons, A. Springer, 1994. doi: 10.1007/978-94-015-8254-4_12.

Toonen, W. H. J., Munoz, S. E., Cohen, K. M., and Macklin, M. G. High-resolution sedimentary paleoflood records in alluvial river environments: A review of recent methodological advances and application to flood hazard assessment. In *Palaeohydrology, Geography of the Physical Environment*, edited by Herget, J. and Fontana, A. Springer, 2019. doi: 10.1007/978-3-030-23315-0_11.

Unde, M. G. and Dhakal, S. Sediment characteristics at river confluences: a case study of the Mula-Kas confluence, Maharashtra, India. *Progress in Physical Geography: Earth and Environment*, 33(2):208–223, 2009. doi: 10.1177/0309133309338655.

USGS National UAS Project Office. Unmanned Aircraft Systems Data Post Processing Structure-from-Motion Photogrammetry, 2017, https://www.usgs.gov/centers/geosciences-and-environmental-change-science-center/science/science-topics/unmanned.

Vidal-Abarca Gutierrez, M. R., Nicolás-Ruiz, N., Sánchez-Montoya, M. d. M., and Suárez Alonso, M. L. Ecosystem services provided by dry river socio-ecological systems and their drivers of change. *Hydrobiologia*, 850(12):2585–2607, 2023. doi: 10.1007/s10750-022-04915-8.

Vyverberg, K. A review of stream processes and forms in dryland watersheds. Technical report, California Department of Fish & Games, 2010.

Wertz, J. B. The flood cycle of ephemeral mountain streams in the southwestern United States. *Annals of the Association of American Geographers*, 56(4):598–633, 1966. doi: 10.1111/j.1467-8306.1966.tb00582.x.

Wheaton, J. M., Brasington, J., Darby, S. E., and Sear, D. A. Accounting for uncertainty in DEMs from repeat topographic surveys: improved sediment budgets. *Earth Surface Processes and Landforms*, 35(2):136–156, 2010. doi: 10.1002/esp.1886.

Zhang, Y., Huang, C. C., Pang, J., Zha, X., Zhou, Y., Yin, S., and Wang, J. Comparative study of the modern flood slackwater deposits in the upper reaches of Hanjiang and Weihe River Valleys, China. *Quaternary International*, 282:184–191, 2012. doi: 10.1016/j.quaint.2012.03.056.

Zituni, R., Greenbaum, N., Porat, N., and Benito, G. Magnitude, frequency and hazard assessment of the largest floods in steep, mountainous bedrock channels of the Southern Judean Desert, Israel. *Journal of Hydrology: Regional Studies*, 37:100886, 2021. doi: 10.1016/j.ejrh.2021.100886.